

Effective one-band models for the 1D cuprate $\text{Ba}_{2-x}\text{Sr}_x\text{CuO}_{3+\delta}$

A. E. Feiguin

Physics Department, Northeastern University, Boston, MA 02115, USA

Christian Helman

*Centro Atómico Bariloche and Instituto Balseiro,
CNEA, GAIDI 8400 S. C. de Bariloche, Argentina*

A. A. Aligia

*Instituto de Nanociencia y Nanotecnología CNEA-CONICET, GAIDI,
Centro Atómico Bariloche and Instituto Balseiro, 8400 Bariloche, Argentina*

We consider a multiband Hubbard model H_m for Cu and O orbitals in $\text{Ba}_{2-x}\text{Sr}_x\text{CuO}_{3+\delta}$ similar to the tree-band model for two-dimensional (2D) cuprates. The hopping parameters are obtained from maximally localized Wannier functions derived from *ab initio* calculations. Using the cell perturbation method, we derive both a generalized $t-J$ model H_{tJ} and a one-band Hubbard model H_H to describe the low-energy physics of the system. H_{tJ} has the advantage of having a smaller relevant Hilbert space, facilitating numerical calculations, while additional terms should be included in H_H to accurately describe the multi-band physics of H_m . Using H_{tJ} and DMRG, we calculate the wave-vector resolved photoemission and discuss the relevant features in comparison with recent experiments. In agreement with previous calculations, we find that the addition of an attractive nearest-neighbor interaction of the order of the nearest-neighbor hopping shifts weight from the $3k_F$ to the holon-folding branch. Kinetic effects also contribute to this process.

I. INTRODUCTION

After more than three decades from the discovery of high- T_c superconductivity, the pairing mechanism is still not fully understood, although it is believed that it is related to spin fluctuations originating from the effective Cu-Cu superexchange J , and complicated by the existence of several phases competing with superconductivity¹⁻⁴. However, there is consensus that for energies below an energy scale of the order of 1 eV, the physics of the two-dimensional (2D) superconducting cuprates is described by the three-band Hubbard model^{5,6} H_{3b} , which contains the $3d_{x^2-y^2}$ orbitals of Cu and the $2p_\sigma$ orbitals of O⁷.

More recently, one-dimensional (1D) cuprates have attracted a great deal of attention, in particular because numerical techniques in 1D are more powerful and also field-theoretical methods like bosonization can be used⁸⁻²⁰. Neudert *et al.* have studied experimentally and theoretically the distribution of holes in the 1D cuprate Sr_2CuO_3 ⁸. The authors discuss several multiband models and the effect of several terms. Recently, angle-resolved photoemission experiments have been carried out in a related doped compound $\text{Ba}_{2-x}\text{Sr}_x\text{CuO}_{3+\delta}$ and analyzed on the basis of a one-band Hubbard model with parameters chosen *ad hoc*¹⁴. The need to add nearest-neighbor attraction or phonons to fit the experiment has been suggested^{14,17,19,20}. Li *et al.* studied a four-band and a one-band Hubbard model and noted that the latter lacks the electron-hole asymmetry observed in resonant inelastic x-ray scattering experiments¹⁶.

The questions we want to address in this work are: 1) which is the appropriate multiband Hubbard model H_m to describe $\text{Ba}_{2-x}\text{Sr}_x\text{CuO}_{3+\delta}$? 2) What are the physical

values of the parameters? 3) To what extent can this model be represented by simpler one-band ones?

Due to the large Hilbert space of H_m , different low-energy reduction procedures have been used to obtain simpler effective Hamiltonians for the 2D cuprates²¹⁻²⁷. Most of them are based on projections of H_m onto the low-energy space of Zhang-Rice singlets (ZRS)²⁸. In spite of some controversy remaining about the validity of this approach²⁹⁻³⁴, the resulting effective models seem to describe well the physics of the 2D cuprates. However, the effect of excited states above the ZRS, often neglected, can have an important role³⁵. For example, if one considers the Hubbard model as an approximation to H_m (as done in Ref. 14), it is known that it leads, in second-order in the hopping t , to a term which in one dimension (1D) takes the form

$$H_{t''} = t'' \sum_{i\sigma} \left(c_{i+2\bar{\sigma}}^\dagger c_{i+1\sigma}^\dagger c_{i+1\bar{\sigma}} c_{i\sigma} - c_{i+2\sigma}^\dagger n_{i+1\bar{\sigma}} c_{i\sigma} + \text{H.c.} \right), \quad (1)$$

with $t'' = t^2/U > 0$, where $n_{i\sigma} = c_{i\sigma}^\dagger c_{i\sigma}$ and $\bar{\sigma} = -\sigma$. This term is an effective *repulsion* and inhibits superconductivity in 1D, while as expected, it favors superconductivity if the sign is changed^{36,37}. Interestingly, some derivations of the generalized $t-J$ model for 2D cuprates suggest that t'' can be negative for some parameters of H_m ^{27,38}, and a very small term $t'' = -t/20$ can have a dramatic effect favoring *d*-wave superconductivity³⁹. Even if the realistic t'' is positive, it is expected to be smaller than that derived from the Hubbard model and might explain why studies of the superconductivity in the one-band Hubbard model conclude that part of the pairing interaction is missing⁴.

Therefore, a discussion on the appropriate model to describe the 1D cuprates and, in particular, $\text{Ba}_{2-x}\text{Sr}_x\text{CuO}_{3+\delta}$ seems necessary. In this work we calculate the hopping parameters of the multiband model for this compound and use this information to derive simpler one-band models.

The paper is organized as follows. In Section II we explain the multiband Hubbard model H_m and derive its hopping parameters using maximally localized Wannier functions (MLWF). In Section III we describe the resulting generalized $t - J$ model obtained from H_m by a low-energy reduction procedure explained briefly in the appendix. In Section IV we explain the corresponding results for the one-band Hubbard model. In Section V we calculate the photoemission spectrum using the time-dependent density-matrix renormalization-group method^{40–43} and we compare it with previous experimental and theoretical results. Section VI contains a summary and discussion.

II. THE MULTIBAND HUBBARD MODEL

We use the following form of the Hamiltonian

$$\begin{aligned}
 H_m = & U_d \sum_i d_{i\uparrow}^\dagger d_{i\uparrow} d_{i\downarrow}^\dagger d_{i\downarrow} + \sum_{i\sigma} \{ \epsilon_{\text{Cu}} d_{i\sigma}^\dagger d_{i\sigma} \\
 & + \frac{\epsilon_{\text{O}}}{2} \sum_{\delta} p_{i+\delta\sigma}^\dagger p_{i+\delta\sigma} + \epsilon_{\text{O}}^{\text{ap}} \sum_{\gamma} p_{i+\gamma\sigma}^\dagger p_{i+\gamma\sigma} \\
 & + [d_{i\sigma}^\dagger (t_{pd}^x \sum_{\delta} p_{i+\delta\sigma} + t_{pd}^y \sum_{\gamma} p_{i+\gamma\sigma}) \\
 & - t_{pp} \sum_{\delta\gamma} p_{i+\delta\sigma}^\dagger p_{i+\gamma\sigma} + \text{H.c.}] \}, \quad (2)
 \end{aligned}$$

where $d_{i\sigma}^\dagger$ ($p_{j\sigma}^\dagger$) creates a hole with spin σ at Cu (O) site i (j). We choose the chain direction as x (a in Fig. 1) and $\delta = \pm a\hat{x}/2$ denote the vectors that connect a Cu atom with their nearest O atoms in the chain direction, where a is the Cu-Cu distance that we take as 1 in what follows. γ has a similar meaning for the apical O atoms, displaced from the chain in the y direction (c in Fig. 1). The relevant O orbitals are those pointing towards their nearest Cu atoms. To simplify the form of the Hamiltonian, we have changed the signs of half of the orbitals in such a way that sign of the hopping terms do not depend on direction and $t_{pd}^x, t_{pd}^y, t_{pp} > 0$ ⁴⁴.

In comparison with previous approaches^{8,16}, two terms are missing: the intratomic O repulsion U_p and the interatomic Cu-O repulsion U_{pd} . Although the former is rather sizeable ($U_p \sim 4$ eV has been estimated in 2D cuprates⁴⁵), we find that it has very little influence on the parameters of the one-band models because of the low probability of double hole occupancy at the O sites. The value of U_{pd} is difficult to determine from spectroscopic measurements⁴⁶ and its effect on different quantities can be absorbed in other parameters⁸. We obtain a

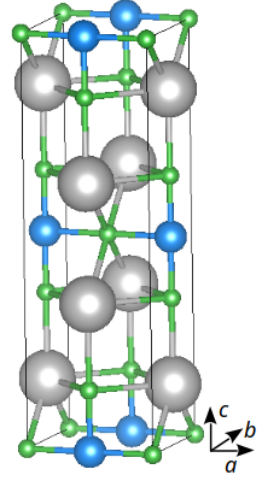


FIG. 1. Unit cell of BaCuO_3 . The gray/blue/green ball are Ba/Cu/O respectively. The lattice parameters are $a = 3.85\text{\AA}$, $b = 4.17\text{\AA}$ and $c = 13.18\text{\AA}$. The CuO chains are along the a direction with distance among them of 4.14\AA .

better agreement with the measured photoemission spectra assuming $U_{pd} = 0$. We also take $U_d = 10$ eV and $\Delta = \epsilon_{\text{O}} - \epsilon_{\text{Cu}} = 3.5$ eV, from calculations in the 2D cuprates⁴⁵ and $\epsilon_{\text{O}}^{\text{ap}} - \epsilon_{\text{O}} = -0.4$ eV was determined as the value that leads to a ratio 1.225 between the occupancy of apical and chain O atoms, very similar to determined experimentally in Sr_2CuO_3 ⁸. The values of the hopping parameters $t_{pd}^x = 1.10$ eV, $t_{pd}^y = 1.04$ eV, and $t_{pp} = 0.60$ eV were determined from density functional theory (DFT) calculations along with the MLWF method.

For the DFT calculations, we use the QUANTUM ESPRESSO code^{47,48}, with the GGA approximation for the exchange and correlation potential and PAW-type pseudopotentials. The energy cut for the plane waves is 80 Ry, and the mesh used in reciprocal space is $15 \times 15 \times 5$. The unit cell is an orthorhombic structure with lattice parameters $a = 3.85\text{\AA}$, $b = 4.17\text{\AA}$ and $c = 13.18\text{\AA}$, and contains two formula units, see Fig. 1.

We consider the spin unpolarized case and obtain the bands shown in Fig. 2. The MLWF procedure involves band fitting of the DFT results, as shown in blue in Fig. 2. The energy window selected to project the Wannier orbital is between 3.75 eV and 10.75 eV, and the orbitals are centered in Cu and O atoms with d and p character, respectively. Other convergence parameters are also successfully evaluated, as suggested in Ref. 49. Finally, the hopping parameters are extracted from the Hamiltonian expressed in the Wannier basis.

III. THE GENERALIZED $t - J$ MODEL

Using the cell-perturbation method^{24,25}, with appropriate modifications for this 1D compound, we find that the system can be described with the following general-

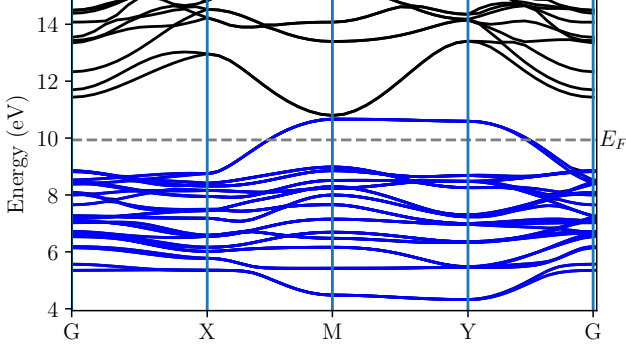


FIG. 2. Band structure for the BaCuO₃ obtained for unpolarized DFT calculation. In blue the bands from the MLWF procedure superposed with DFT ones.

ized $t - J$ model

$$\begin{aligned}
 H_{tJ} = & -t \sum_{i\sigma} \left(c_{i\sigma}^\dagger c_{i+1\sigma} + \text{H.c.} \right) \\
 & -t_2 \sum_{i\sigma} \left(c_{i\sigma}^\dagger c_{i+2\sigma} + \text{H.c.} \right) \\
 & + \sum_i (J \mathbf{S}_i \cdot \mathbf{S}_{i+1} + V n_i n_{i+1}) + H_{t''}, \quad (3)
 \end{aligned}$$

with $t_2 = t/5$. Minor terms of magnitude below 0.04 eV were neglected. The parameters of the model are given by analytical expressions in terms of the eigenstates and energies of a cell Hamiltonian, that are obtained after solving a 6×6 matrix and two 3×3 matrices. A summary of the method is included in the appendix.

For the parameters of the multiband model described above, we obtain $t = 0.443$ eV, $J = 0.314$ eV, $V = -0.143$ eV, and $t'' = 0.068$ eV. Interestingly, our values for J and t'' without adjustable parameters are similar to those corresponding to the Hubbard model chosen to explain the experiments by Chen *et al.*¹⁴.

The larger values of t and J compared to the 2D cuprates (for example $t = 0.37$ meV, $J = 0.15$ meV for T-CuO³²) are expected due to the larger overlap between the normalized O orbitals $\sum_{\delta} p_{i+\delta\sigma}$ that hybridize with the Cu for nearest-neighbor Cu positions. This leads to a larger overlap between non-orthogonal ZRS^{27,50} and to a larger extension of the orthogonal oxygen Wannier functions centered at the Cu sites (see appendix). For Sr₂CuO₃, the reported values of $J \sim 0.24$ meV⁸⁻¹² are also larger than those of 2D cuprates. The resulting value of t is somewhat smaller than that used in Ref. 14 but is compensated by the hopping to second nearest neighbors.

The fact that the nearest-neighbor attraction V is larger than $J/4$ as expected for the mapping from the Hubbard to the $t - J$ model is due to the contribution of excited local triplets absent in the Hubbard model.

For other parameters of H_m , in particular increasing the ratio t_{pp}/t_{pd} and the difference between O and Cu on-site energies, t'' changes sign as expected from calculations in 2D cuprates^{27,38}. For example increasing t_{pp} to 1 eV and both on-site energy differences to 7 eV (unrealistic for Ba_{2-x}Sr_xCuO_{3+δ} but near to the values expected for nickelates), we obtain $t = 0.531$ eV, $J = 0.105$ eV, $V = -0.096$ eV, and $t'' = -0.019$ eV, due to the increasing relative importance of excited triplets.

IV. THE EFFECTIVE ONE-BAND HUBBARD MODEL

The generalized $t - J$ model discussed above describes the movement of ZRS (two-hole states) in a chain of singly occupied cells. If the cells with no holes are also considered (because for example one is interested in larger energy scales), one can also derive a one-band Hubbard-like model using the cell perturbation method. A simple version of this model has the form²¹⁻²³

$$\begin{aligned}
 H_H = & -t \sum_{i\sigma} \left(c_{i\sigma}^\dagger c_{i+1\sigma} + \text{H.c.} \right) [t_{AA}(1 - n_{i\bar{\sigma}})(1 - n_{i+1\bar{\sigma}}) \\
 & + t_{BB}n_{i\bar{\sigma}}n_{i+1\bar{\sigma}} + t_{AB}(n_{i\bar{\sigma}} + n_{i+1\bar{\sigma}} - 2n_{i\bar{\sigma}}n_{i+1\bar{\sigma}})] \\
 & + U \sum_i n_{i\uparrow}n_{i\downarrow}. \quad (4)
 \end{aligned}$$

As for H_{tJ} , we map the ZRS into empty states of H_H . Then t_{AA} coincides with t of H_{tJ} . From the mapping procedure we obtain $t_{AA} = 0.443$ eV, $t_{AB} = 0.421$ eV, $t_{BB} = 0.369$ eV, and $U = 2.083$ eV. The model is electron-hole symmetric if and only if $t_{AA} = t_{BB}$, while the photoemission of H_m is asymmetric in general¹⁶.

Another shortcoming of H_H is that if the model is reduced to a generalized $t - J$ one by eliminating double occupied sites, the effective $J = 4t_{AB}^2/U = 0.376$ eV and $t'' = J/4 = 0.094$ eV are overestimated with respect to the values obtained in the previous section: $J = 0.314$ eV, and $t'' = 0.068$ eV. Instead, the NN attraction $-J/4$ is underestimated ($V = -0.143$ eV above). This is due to the neglect of the triplets in H_H (see appendix and Ref. 38). Therefore H_{tJ} is more realistic to describe the photoemission spectrum of hole doped 1D cuprates, unless additional terms are added to H_H .

V. PHOTOEMISSION SPECTRUM OF H_{tJ}

A. Photoemission intensity as a function of wave vector

While the effective Hamiltonian H_{tJ} is enough to accurately describe the *energy spectrum* of H_m at low energies, this is not the case for the spectral *intensity* since one needs to map the *operators* for the creation of Cu and

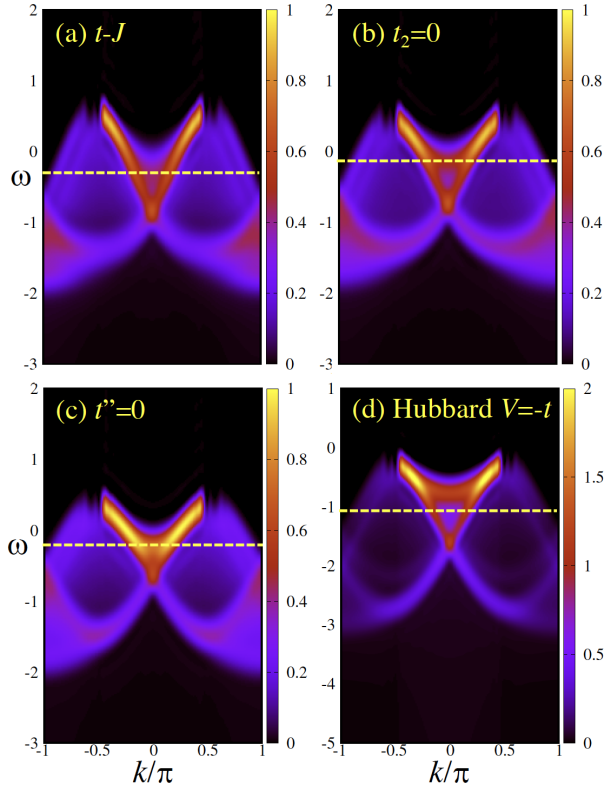


FIG. 3. Photoemission spectrum of (a) the generalized $t-J$, Eq. 3; (b) same but setting the second-neighbor hopping to zero; (c) $t'' = 0$. Panel (d) shows results for the extended Hubbard model with $t = 0.6$, $U/t = 8$; $V/t = -1$ for comparison.

O holes in H_m to the corresponding ones of the effective low-energy Hamiltonian that one uses^{51,52}

In the 2D cuprates, it has been found by numerical diagonalization of small clusters, that the photoemission intensity due to O atoms at low energies can be well approximated by the expression⁵²

$$I_O = 1.22 \times Z(\mathbf{k})[\sin^2(k_x/2) + \sin^2(k_y/2)], \quad (5)$$

where $Z(\mathbf{k})$ is the quasiparticle weight of the generalized $t-J$ model. The dependence on wave vector can be understood from the fact that at $k = 0$, the O states which point towards their nearest Cu atoms are odd under reflection through the planes perpendicular to the orbitals, while the low-energy orbitals that form the ZRS are even under those reflections. Comparison of this expression to experiment is very good³⁰. A variational treatment of a spin-fermion model for the cuprates also leads to a vanishing weight at $k_x = k_y = 0$ ²⁹. A similar dependence is expected in the 1D case due to the contribution of the O orbitals along the chain, which increases the relative weight for $k_x \sim \pi/2$. To estimate the relative weight due to these orbitals, we have calculated the probability of creating a hole $(e^{ik}p_{i+\delta}^\dagger - p_{i-\delta}^\dagger)/\sqrt{2}$ (the minus sign is due to the choice of phases in H_m) in a singly occupied

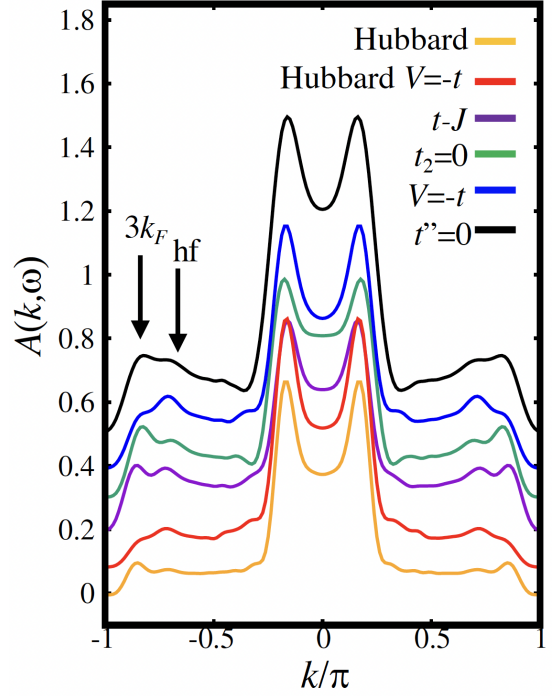


FIG. 4. Momentum distribution curves: cuts along the fixed frequency dashed lines in Fig. 3. The features corresponding to the holon-folding (hf) and $3k_F$ bands are highlighted by arrows. The curves are ordered from bottom to top and shifted 0.1 up in intensity from the previous one for clarity.

cell leaving a ZRS, and also the corresponding result for apical O and Cu.

In addition, the observed total intensity depends on the cross sections f for Cu and O, which in turn depend sensitively on the frequency of the radiation used. The ratio of cross sections for the reported energy (65 eV) of the x-ray beam (available at <https://vuo.elettra.eu/>) is $f_{\text{Cu}}/f_{\text{O}} = 3.077$. Using this result and the above mentioned probabilities for the parameters of H_m described in the previous Section, we obtain that the wave vector dependence of the photoemission intensity can be written as

$$I(k) \sim Z(k)[A + B \sin^2(k/2)], \quad (6)$$

where $Z(k)$ is the quasiparticle weight of the generalized $t-J$ model, and $A = 1.097$ and $B = 0.205$.

B. Numerical results

We calculated the photoemission spectrum of the generalized $t-J$ model using time-dependent density-matrix renormalization group (tDMRG)^{40,41,43,53}. The simulation yields the single particle two-time correlator $G(x, t) = i\langle c_\sigma^\dagger(x, t)c_\sigma(L/2, 0) \rangle$. This is Fourier transformed to frequency and momentum, allowing

one to retrieve the spectral function as $A(k, \omega) = -\text{Im}G(k, \omega)/\pi$. The method has been extensively described elsewhere^{43,53} and we hereby mention some (standard) technical aspects. Simulations are carried out using a time-targeting scheme with a Krylov expansion of the evolution operator⁴². Since open boundary conditions are enforced and the chain length is even, the correlations in real space are symmetrized with respect to the “midpoint” $x = L/2$. In order to reduce boundary effects we convolve $G(x, t)$ with a function that decays smoothly to zero at the ends of the chain and at long times, automatically introducing an artificial broadening. The function of choice is the so-called “Hann window” $(1 + \cos(x\pi/\sigma))/2$, where σ is the window width. We apply this window to the first and last quarter of the chain. We study systems of length $L = 80$ sites, and $N = 74$ electrons, corresponding to a 7.5% doping, using $m = 600$ DMRG states (guaranteeing a truncation error below 10^{-6}), a time step $\delta t = 0.05$ and a maximum time $\sigma = t_{\text{max}} = 20$. This density is chosen to maximize the holon folding (hf) effect discussed in Ref. 14.

Due to the one-dimensionality, the low-energy physics of the models discussed here falls into the universal class of Luttinger liquid theory^{54–57}. Accordingly, excitations are not full-fledged Landau quasi-particles and the spectrum displays edge singularities instead of Lorentzians. In addition, and most remarkably, they realize the phenomenon known as spin-charge separation, with independent charge and spin excitations that propagate with different velocities and characteristic energy scales: the spinon bandwidth is determined by J , while the holon bandwidth by the hopping t . In the photoemission spectrum, these excitations appear as separate branches between $-k_F$ and k_F , with the spinon branch looking like an arc connecting the two points. Unlike non interacting systems, the photoemission spectrum extends beyond $|k| > k_F$ due to momentum transfer between spinons and holons: An electron with energy $\epsilon(k)$ can fractionalize into spin and charge excitations such that $\epsilon_s(q) + \epsilon_c(k - q) = \epsilon(k)$, leading to a high energy continuum and additional branches leaking out from $k = \pm k_F$ and $k = \pm 3k_F$ ^{58–60} (the first one is referred to as the holon-folding band in Ref. 14 and as “shadow bands” in Ref. 61).

Results for the generalized $t - J$ model [Eq. (3)] are shown in Fig. 3(a) for the physical parameters corresponding to $\text{Ba}_{2-x}\text{Sr}_x\text{CuO}_{3+\delta}$, as discussed above. To understand the contributions of the different terms we also considered the cases without second-neighbor hopping in Fig. 3(b), and without correlated hopping ($t'' = 0$), Fig. 3(c). In all these curves, the spectral density has been rescaled according to Eq. (6). As a reference, we also show results for the extended Hubbard chain with $U = 8t$ and second neighbor attraction $V = -t$ ($t = 0.6eV$).

We notice that the Hubbard chain has more spectral weight concentrated on the holon branches, while in the $t - J$ model it is more distributed in the continuum and

even in the continuation of the holon bands at high energies. In addition, we observe that the $t - J$ model has a larger spinon velocity with a wider spinon branch, and a larger charge velocity with a holon band $\sim 20\%$ wider than the one for the Hubbard model (we measure the holon bandwidth as the distance between the Fermi energy and the crossing of the two holon branches at $k = 0$). Since the value of J remains unchanged, we attribute these effects to kinematic sources (the extra hopping terms).

In order to compare to previous attempts to interpret the experimental observations, we analyze momentum distribution curves at fixed frequency values, plotted in Fig. 4, corresponding to the yellow dashed lines in Fig. 3. We include results for the extended Hubbard model with $U/t = 8, V = -t$ and $V = 0$, that agree very well with similar previous calculations^{17,19}. Note that the parameters of this Hubbard model are not those that correspond to the mapping discussed in section IV, but the chosen value of U gives rise to an effective J similar to the correct one. In this figure it is easier to observe the signatures of the k_F and $3k_F$ holon branches at high momentum, which are quite faint in the color density plot and are highlighted here with arrows. One can also appreciate the qualitative differences between the extended Hubbard model with $V = -t$ and the other cases. In particular, by comparing to the standard Hubbard model with $V = 0$ we notice a transfer of weight from the edge of the continuum ($3k_F$ -band) to the holon-folding band, which in Ref. 14 is attributed to a phonon induced attraction. On the other hand, the $t - J$ model realizes a more prominent feature at $3k_F$ and the hf-band, and the continuum contains markedly more spectral weight in the sidebands than the Hubbard model. We also include results for the generalized $t - J$ model with $V = -t$ and we observe results practically identical to those for the extended Hubbard model with attraction.

Our results indicate that there are both kinetic as well as many-body effects that affect the relative spectral weight concentrated in the sidebands: While t_2 and t'' shift weight from the center toward the folding and $3k_F$ bands, the attraction V shifts weight toward the center and from the $3k_F$ band into the holon-folding (hf) one. However, comparing with the cases of vanishing t_2 and t'' , we see that these terms also have an effect of shifting weight from the $3k_F$ to the hf band but of smaller magnitude.

VI. SUMMARY AND DISCUSSION

We have started our description of CuO_3 chains of $\text{Ba}_{2-x}\text{Sr}_x\text{CuO}_{3+\delta}$ from a four-band model (with one relevant orbital per Cu or O atom). The hopping parameters of the model were obtained using maximally localized Wannier functions. Extending the cell-perturbation method used for CuO_2 planes of the superconducting cuprates to this one-dimensional compound, we derive

simpler one-band models that are more amenable to numerical techniques due to the smaller Hilbert space. In order to account for the effect of excited triplets, the one-band Hubbard model should be supplemented by other terms not usually considered. In addition the hopping term depends on the occupancy of the sites involved. For energies below the value of the effective Coulomb repulsion U , it is more convenient to use the generalized $t-J$ model.

We have calculated the photoemission spectrum of this model using time-dependent density-matrix renormalization group. The results are in semiquantitative agreement with experiment. We obtain that the hopping to second nearest-neighbors and the three-site term $H_{t''}$ have a moderate effect in shifting weight from the $3k_F$ peak to the holon-folding branch, but a nearest-neighbor attraction has a stronger effect. For energies below U and if only either electron or hole doping is of interest, a Hubbard model with an artificially enlarged U that leads to the correct value of the effective nearest-neighbor exchange J , shows a photoemission spectrum very similar to the corresponding results for the generalized $t-J$ model.

ACKNOWLEDGMENTS

We thank Alberto de la Torre and Giorgio Levy for information regarding Cu and O cross sections for photoionization. We enjoyed fruitful discussions with Alberto Nocera, Steven Johnston and Yao Wang. AAA acknowledges financial support provided by PICT 2017-2726 and PICT 2018-01546 of the ANPCyT, Argentina. AEF acknowledges support from the U.S. Department of Energy, Office of Basic Energy Sciences under grant No. DE-SC0014407. CH acknowledges financial support provided by PICT 2019-02665 of the ANPCyT, Argentina.

Appendix A: Derivation of the effective one-band models

Here we summarize the application of the cell-perturbation method^{24,25}, to the case of the one-dimensional compound.

The Cu orbitals at each site are hybridized with symmetric linear combinations of O orbitals of the form (dropping for the moment the spin subscripts)

$$a_i^\dagger = \frac{p_{i+\gamma}^\dagger + p_{i-\gamma}^\dagger}{\sqrt{2}}, q_i^\dagger = p_{i+\delta}^\dagger + p_{i-\delta}^\dagger, \quad (\text{A1})$$

To change the basis of the q_i^\dagger to orthonormal Wannier functions²⁸, we Fourier transform

$$q_k^\dagger = \frac{1}{\sqrt{N}} \sum_l e^{-ikl} q_l^\dagger = \frac{2 \cos(k\delta)}{\sqrt{N}} \sum_j e^{-ikj} p_j^\dagger, \quad (\text{A2})$$

where the sum over $l(j)$ runs over all Cu(O) sites. The operators

$$\pi_k^\dagger = \frac{1}{2|\cos(k\delta)|} q_k^\dagger, \quad (\text{A3})$$

satisfy $\{\pi_{k_1}^\dagger, \pi_{k_2}\} = \delta_{k_1, k_2}$. Transforming to real space one obtains the Wannier O orbitals centered at the Cu sites

$$\pi_l^\dagger = \frac{1}{\sqrt{N}} \sum_k e^{ikl} \pi_k^\dagger = \sum_j A(l-j) p_j^\dagger, \\ A(j) = \frac{1}{N} \sum_k e^{ikj} \text{sgn}[\cos(k\delta)] = \frac{(-1)^{j-1/2}}{j\pi}. \quad (\text{A4})$$

Changing the basis of the O orbitals, the hopping terms in the Hamiltonian Eq. (2) (those proportional to $t_{pd}^x, t_{pd}^y, t_{pp}$) that act inside each cell that includes a Cu site and the O Wannier functions centered at the same site, becomes

$$H_{\text{hop}}^{\text{intra}} = \sum_{i\sigma} [d_{i\sigma}^\dagger (V_x \pi_{i\sigma} + V_y a_{i\sigma}) + V_O \pi_{i\sigma}^\dagger a_{i\sigma} + \text{H.c.}], \\ V_x = 2A(1/2)t_{pd}^x, \quad V_y = \sqrt{2}t_{pd}^y, \\ V_O = -2\sqrt{2}A(1/2)t_{pp}, \quad (\text{A5})$$

while the remaining part of the hopping takes the form

$$H_{\text{hop}}^{\text{inter}} = \sum_{i\sigma} \sum_{l \neq 0} B_l [\pi_{i+l\sigma}^\dagger (t_{pd}^x d_{i\sigma} - \sqrt{2}t_{pp} a_{i\sigma}) + \text{H.c.}], \\ B_l = A(l+1/2) + A(l-1/2). \quad (\text{A6})$$

The on-site terms of H_{3b} retain the same form. This part and $H_{\text{hop}}^{\text{intra}}$ is solved exactly in the subspaces of one and two holes. For one hole and given spin, one has a 3×3 matrix, and we denote as E_1 the lowest energy in this subspace. For two holes and neglecting U_p there is a 6×6 matrix for the singlet states and a 3×3 matrix for each spin projection of the triplet states. The ground state of the subspace of singlets with energy E_s is identified as the Zhang-Rice singlet (ZRS)²⁸ and mapped into an empty site in the effective generalized $t-J$ model. The Coulomb repulsion in the effective Hubbard model is $U = E_s - 2E_1$.

An advantage of the cell perturbation method is that most of the hopping terms are included in $H_{\text{hop}}^{\text{intra}}$ and including exactly in these matrices. The rest of the hopping $H_{\text{hop}}^{\text{inter}}$ is treated in perturbation theory. The first-order correction gives rise to effective hopping at different distances. An important difference with the two-dimensional case is that the larger overlap between linear combinations of the original O orbitals centered at a Cu site [as the q_i^\dagger in Eq. (A1)] leads to larger effective hoppings and to a slower decay with distance. Note that the ratio of second nearest-neighbor (NN) hopping to the

first NN one is $t_2/t_1 = -B_2/B_1 = 1/5$ (the minus sign comes from restoring the original signs of half of the orbitals, which have been changed to simplify H_{3b}) and for third NN $t_3/t_1 = B_3/B_1 = 3/35$ (these ratios change if corrections due to U_p and U_{pd} are included).

In the effective Hubbard model, there are actually three different hopping terms depending on the occupancy of the sites involved, while in the generalized $t - J$ model, only the one related with the exchange of Zhang-Rice singlets with singly occupied sites is important.

The most important second-order corrections in $H_{\text{hop}}^{\text{inter}}$ lead to a superexchange J and nearest-neighbor attraction $-V$ in the generalized $t - J$ model. For example, one of these second-order processes leads to an effective spin-flip process between a state with one hole with spin \uparrow at site i and another with spin \downarrow at site $i + 1$, and another one with the spins interchanged, through an intermediate state with no holes at site i and two holes at site $i + 1$. While the states with one hole correspond to

the ground state of the above mentioned 3×3 matrix, the two-hole part of the intermediate states include all singlet and triplet states of the corresponding 6×6 and 3×3 matrices. This is an important difference with the Hubbard model, because in the latter, only the ground state of the 6×6 matrix of singlets is included in the effective exchange $J_H = 4t_{AB}^2/U$ and the triplets are neglected, leading to an overestimation of J_H , because the contribution of the triplets is negative.

The next important second-order corrections in $H_{\text{hop}}^{\text{inter}}$ correspond to three-site terms. They lead for example to an effective mixing between states with one hole at sites i and $i + 1$ and a ZRS at site $i + 2$ and states with a ZRS at site i and one hole at sites $i + 1$ and $i + 2$. As before, performing second-order perturbation theory in the Hubbard model includes only a few of these contributions.

The different terms can be expressed analytically in terms of the eigenstates and eigenenergies of the matrices of the local cell mentioned above. The expressions are lengthy and are not reproduced here.

-
- ¹ B. Keimer, S. A. Kivelson, M. R. Norman, S. Uchida, and J. Zaanen, *Nature* **518**, 179 (2015).
 - ² E. Fradkin, S. A. Kivelson, and J. M. Tranquada, *Rev. Mod. Phys.* **87**, 457 (2015).
 - ³ S. M. O'Mahony, W. Ren, W. Chen, Y. X. Chong, X. Liu, H. Eisaki, S. Uchida, M. H. Hamidian, and J. C. S. Davis, *Proceedings of the National Academy of Sciences* **119**, e2207449119 (2022).
 - ⁴ X. Dong, E. Gull, and A. J. Millis, *Nature Physics* **18**, 1293 (2022).
 - ⁵ C. Varma, S. Schmitt-Rink, and E. Abrahams, *Solid State Communications* **62**, 681 (1987).
 - ⁶ V. J. Emery, *Phys. Rev. Lett.* **58**, 2794 (1987).
 - ⁷ To explain some Raman and photoemission experiments at higher energies, other orbitals should be included (see for example Ref. ?), but we can neglect them in this work).
 - ⁸ R. Neudert, S.-L. Drechsler, J. Málek, H. Rosner, M. Kielsch, Z. Hu, M. Knupfer, M. S. Golden, J. Fink, N. Nücker, M. Merz, S. Schuppler, N. Motoyama, H. Eisaki, S. Uchida, M. Domke, and G. Kaindl, *Phys. Rev. B* **62**, 10752 (2000).
 - ⁹ I. A. Zalitznyak, H. Woo, T. G. Perring, C. L. Broholm, C. D. Frost, and H. Takagi, *Phys. Rev. Lett.* **93**, 087202 (2004).
 - ¹⁰ B. J. Kim, H. Koh, E. Rotenberg, S. J. Oh, H. Eisaki, N. Motoyama, S. Uchida, T. Tohyama, S. Maekawa, Z. X. Shen, and C. Kim, *Nature Physics* **2**, 397 (2006).
 - ¹¹ A. C. Walters, T. G. Perring, J.-S. Caux, A. T. Savici, G. D. Gu, C.-C. Lee, W. Ku, and I. A. Zalitznyak, *Nature Physics* **5**, 867 (2009).
 - ¹² J. Schlappa, K. Wohlfeld, K. J. Zhou, M. Mourigal, M. W. Haverkort, V. N. Strocov, L. Hozoi, C. Monney, S. Nishimoto, S. Singh, A. Revcolevschi, J. S. Caux, L. Patthey, H. M. Rønnow, J. van den Brink, and T. Schmitt, *Nature* **485**, 82 (2012).
 - ¹³ K. Wohlfeld, S. Nishimoto, M. W. Haverkort, and J. van den Brink, *Phys. Rev. B* **88**, 195138 (2013).
 - ¹⁴ Z. Chen, Y. Wang, S. N. Rebec, T. Jia, M. Hashimoto, D. Lu, B. Moritz, R. G. Moore, T. P. Devereaux, and Z.-X. Shen, *Science* **373**, 1235 (2021), <https://www.science.org/doi/pdf/10.1126/science.abf5174>.
 - ¹⁵ H.-S. Jin, W. E. Pickett, and K.-W. Lee, *Phys. Rev. B* **104**, 054516 (2021).
 - ¹⁶ S. Li, A. Nocera, U. Kumar, and S. Johnston, *Communications Physics* **4**, 217 (2021).
 - ¹⁷ Y. Wang, Z. Chen, T. Shi, B. Moritz, Z.-X. Shen, and T. P. Devereaux, *Phys. Rev. Lett.* **127**, 197003 (2021).
 - ¹⁸ D.-W. Qu, B.-B. Chen, H.-C. Jiang, Y. Wang, and W. Li, *Communications Physics* **5**, 257 (2022).
 - ¹⁹ T. Tang, B. Moritz, C. Peng, Z. X. Shen, and T. P. Devereaux, "Traces of electron-phonon coupling in one-dimensional cuprates," (2022).
 - ²⁰ H.-X. Wang, Y.-M. Wu, Y.-F. Jiang, and H. Yao, "Spectral properties of 1d extended hubbard model from bosonization and time-dependent variational principle: applications to 1d cuprate," (2022).
 - ²¹ H.-B. Schüttler and A. J. Fedro, *Phys. Rev. B* **45**, 7588 (1992).
 - ²² M. Simon, M. Balina, and A. Aligia, *Physica C: Superconductivity* **206**, 297 (1993).
 - ²³ M. E. Simón and A. A. Aligia, *Phys. Rev. B* **48**, 7471 (1993).
 - ²⁴ L. F. Feiner, J. H. Jefferson, and R. Raimondi, *Phys. Rev. B* **53**, 8751 (1996).
 - ²⁵ V. I. Belinicher, A. L. Chernyshev, and L. V. Popovich, *Phys. Rev. B* **50**, 13768 (1994).
 - ²⁶ V. I. Belinicher and A. L. Chernyshev, *Phys. Rev. B* **49**, 9746 (1994).
 - ²⁷ A. A. Aligia, M. E. Simón, and C. D. Batista, *Phys. Rev. B* **49**, 13061 (1994).
 - ²⁸ F. C. Zhang and T. M. Rice, *Phys. Rev. B* **37**, 3759 (1988).
 - ²⁹ H. Ebrahimnejad, G. A. Sawatzky, and M. Berciu, *Nature Physics* **10**, 951 (2014).
 - ³⁰ I. J. Hamad, L. O. Manuel, and A. A. Aligia, *Phys. Rev. B* **103**, 144510 (2021).
 - ³¹ C. P. J. Adolphs, S. Moser, G. A. Sawatzky, and M. Berciu, *Phys. Rev. Lett.* **116**, 087002 (2016).

- ³² I. J. Hamad, L. O. Manuel, and A. A. Aligia, *Phys. Rev. Lett.* **120**, 177001 (2018).
- ³³ M. Jiang, M. Moeller, M. Berciu, and G. A. Sawatzky, *Phys. Rev. B* **101**, 035151 (2020).
- ³⁴ A. A. Aligia, *Phys. Rev. B* **102**, 117101 (2020).
- ³⁵ S. Li, A. Nocera, U. Kumar, and S. Johnston, *Communications Physics* **4**, 217 (2021).
- ³⁶ B. Ammon, M. Troyer, and H. Tsunetsugu, *Phys. Rev. B* **52**, 629 (1995).
- ³⁷ F. Lema, C. Batista, and A. Aligia, *Physica C: Superconductivity* **259**, 287 (1996).
- ³⁸ M. E. Simón and A. A. Aligia, *Phys. Rev. B* **52**, 7701 (1995).
- ³⁹ C. D. Batista, L. O. Manuel, H. A. Ceccatto, and A. A. Aligia, *Europhysics Letters* **38**, 147 (1997).
- ⁴⁰ S. R. White and A. E. Feiguin, *Phys. Rev. Lett.* **93**, 076401 (2004).
- ⁴¹ A. J. Daley, C. Kollath, U. Schollwöck, and G. Vidal, *Journal of Statistical Mechanics: Theory and Experiment* **2004**, P04005 (2004).
- ⁴² A. E. Feiguin and S. R. White, *Phys. Rev. B* **72**, 020404 (2005).
- ⁴³ S. Paeckel, T. Köhler, A. Swoboda, S. R. Manmana, U. Schollwöck, and C. Hubig, *Annals of Physics* **411**, 167998 (2019).
- ⁴⁴ See for example red orbitals in Fig. S1 of the supplemental material of. Ref. 32.
- ⁴⁵ M. S. Hybertsen, M. Schlüter, and N. E. Christensen, *Phys. Rev. B* **39**, 9028 (1989).
- ⁴⁶ K. Sheshadri, D. Malterre, A. Fujimori, and A. Chainani, *Phys. Rev. B* **107**, 085125 (2023).
- ⁴⁷ P. Giannozzi, S. Baroni, N. Bonini, M. Calandra, R. Car, C. Cavazzoni, D. Ceresoli, G. L. Chiarotti, M. Cococcioni, I. Dabo, A. D. Corso, S. de Gironcoli, S. Fabris, G. Fratesi, R. Gebauer, U. Gerstmann, C. Gougoussis, A. Kokalj, M. Lazzeri, L. Martin-Samos, N. Marzari, F. Mauri, R. Mazzarello, S. Paolini, A. Pasquarello, L. Paulatto, C. Sbraccia, S. Scandolo, G. Sclauszero, A. P. Seitsonen, A. Smogunov, P. Umari, and R. M. Wentzcovitch, *Journal of Physics: Condensed Matter* **21**, 395502 (2009).
- ⁴⁸ P. Giannozzi, O. Andreussi, T. Brumme, O. Bunau, M. B. Nardelli, M. Calandra, R. Car, C. Cavazzoni, D. Ceresoli, M. Cococcioni, N. Colonna, I. Carnimeo, A. D. Corso, S. de Gironcoli, P. Delugas, R. A. DiStasio, A. Ferretti, A. Floris, G. Fratesi, G. Fugallo, R. Gebauer, U. Gerstmann, F. Giustino, T. Gorni, J. Jia, M. Kawamura, H.-Y. Ko, A. Kokalj, E. Küçükbenli, M. Lazzeri, M. Marsili, N. Marzari, F. Mauri, N. L. Nguyen, H.-V. Nguyen, A. O. de-la Roza, L. Paulatto, S. Poncé, D. Rocca, R. Sabatini, B. Santra, M. Schlipf, A. P. Seitsonen, A. Smogunov, I. Timrov, T. Thonhauser, P. Umari, N. Vast, X. Wu, and S. Baroni, *Journal of Physics: Condensed Matter* **29**, 465901 (2017).
- ⁴⁹ G. Pizzi, V. Vitale, R. Arita, S. Blügel, F. Freimuth, G. Géranton, M. Gibertini, D. Gresch, C. Johnson, T. Koretsune, J. Ibañez-Azpiroz, H. Lee, J.-M. Lihm, D. Marchand, A. Marrazzo, Y. Mokrousov, J. I. Mustafa, Y. Nohara, Y. Nomura, L. Paulatto, S. Poncé, T. Ponweiser, J. Qiao, F. Thöle, S. S. Tsirkin, M. Wierzbowska, N. Marzari, D. Vanderbilt, I. Souza, A. A. Mostofi, and J. R. Yates, *Journal of Physics: Condensed Matter* **32**, 165902 (2020).
- ⁵⁰ F. C. Zhang, *Phys. Rev. B* **39**, 7375 (1989).
- ⁵¹ M. Hirayama, T. Misawa, T. Ohgoe, Y. Yamaji, and M. Imada, *Phys. Rev. B* **99**, 245155 (2019).
- ⁵² J. Eroles, C. D. Batista, and A. A. Aligia, *Phys. Rev. B* **59**, 14092 (1999).
- ⁵³ A. E. Feiguin, in *XV Training Course in the Physics of Strongly Correlated Systems*, Vol. 1419 (AIP Proceedings, 2011) p. 5.
- ⁵⁴ T. Giamarchi, *Quantum Physics in One Dimension* (Clarendon Press, Oxford, 2004).
- ⁵⁵ A. O. Gogolin, A. A. Nersisyan, and A. M. Tsvelik, *Bosonization and Strongly Correlated Systems* (Cambridge University Press, Cambridge, England, 1998).
- ⁵⁶ F. Essler, H. Frahm, F. Göhmann, A. Klümper, and V. E. Korepin, *The One-Dimensional Hubbard Model* (Cambridge University Press, Cambridge, England, 2010).
- ⁵⁷ F. D. M. Haldane, *J. Phys. C* **14**, 2585 (1981).
- ⁵⁸ M. Ogata and H. Shiba, *Phys. Rev. B* **41**, 2326 (1990).
- ⁵⁹ K. Penc, K. Hallberg, F. Mila, and H. Shiba, *Phys. Rev. B* **55**, 15475 (1997).
- ⁶⁰ H. Benthien and E. Jeckelmann, *Phys. Rev. B* **75**, 205128 (2007).
- ⁶¹ J. Favand, S. Haas, K. Penc, F. Mila, and E. Dagotto, *Phys. Rev. B* **55**, R4859 (1997).